

# ELECTRIC FIELD AND VOLTAGE DISTRIBUTION ALONG NON-CERAMIC INSULATORS

**Abstract:** The electric field and voltage distribution (EFVD) in the vicinity of non-ceramic insulators is presented. A three-dimensional electric field analysis program, COULOMB, has been used for the calculations. Computation model development and EFVD results are presented for various examples: dry and clean insulators, 765 kV power line insulators, the effect of water droplets, and insulators under rain and fog conditions.

## Integrated Engineering Software - Website Links

[Home](#)

[Products](#)

[Support](#)

[Technical Papers](#)

*"Page Down" or use scroll bars to read the article*

# ELECTRIC FIELD AND VOLTAGE DISTRIBUTION ALONG NON-CERAMIC INSULATORS

Weiguo Que\* and Stephen A. Sebo

Department of Electrical Engineering, The Ohio State University  
Columbus, Ohio 43210, U.S.A. (\*presently with Axcelis Technologies)

**Abstract:** The electric field and voltage distribution (EFVD) in the vicinity of non-ceramic insulators is presented. A three-dimensional electric field analysis program, COULOMB, has been used for the calculations. Computation model development and EFVD results are presented for various examples: dry and clean insulators, 765 kV power line insulators, the effect of water droplets, and insulators under rain and fog conditions.

## 1. INTRODUCTION

Non-ceramic insulators are exposed to various environmental stresses, which include many forms of precipitation, UV radiation, and pollution. The performance of non-ceramic insulators is important for both dry and wet conditions. Long-term problems with them are related to the degradation of polymer materials used for the insulator, corona phenomena on the insulator surface, and pollution flashover. Most of these problems are related to the electric field distribution along the insulators.

The electric field strength on non-ceramic insulators need to be controlled for two reasons:

1. To prevent significant discharge activity on the surface material of non-ceramic insulators under both dry and wet conditions which may result in the degradation of the pollution performance of these insulators.
2. To avoid the internal discharge activity inside the fiberglass rod and the sheath rubber material that could result in mechanical or electrical failure.

When non-ceramic insulators are installed on a three phase power line, the conductors, the hardware, the tower configuration and the presence of the other two phases of the three phase system can influence the electric field strength in the vicinity of the non-ceramic insulators. Therefore, it is important to study these effects from a practical standpoint. To control the electric field strength, the end fitting shape of non-ceramic insulators need to be carefully designed. If necessary, a grading ring needs to be added.

Under rain and fog conditions, non-ceramic insulators become moist or wet under rain and fog conditions. The presence of water droplets causes electric field enhancement. If the magnitude of the surface electric field strength exceeds a threshold value, 0.5-0.7 kV<sub>rms</sub>/mm [1], water droplet corona discharges may occur. The discharges usually occur between water droplets and destroy the hydrophobicity of the polymer material surface. The high temperature of such discharges also thermally degrades the insulator surface. As a consequence, the surface corona discharges from water droplets accelerate the aging of the polymer material, cause surface damage due to tracking and erosion, and increase the risk of the flashover of the non-ceramic insulator.

To study the electric field strength distribution along insulators, there are several numerical analysis methods. There are two different kinds of numerical analysis methods,

using either differential equations or integral equations. The former is known as the “field” approach or domain method, and the second is known as the source distribution technique or boundary method. The domain methods include the finite difference method (FDM) and finite element method (FEM), which apply mainly for domains with bounded boundaries. The boundary method include the charge simulation method (CSM), and the boundary element method (BEM) which apply for domains with open boundaries and have no restrictions in regards the geometry of the domain. For the studies described in this paper, the commercially available program COULOMB, based on the boundary element method, developed by Integrated Engineering Software, has been employed.

The objective of this paper is to study the electric field and voltage distribution (EFVD) along non-ceramic insulators, first, under dry and clean conditions and then under various wet conditions.

## 2. INSULATOR COMPUTATION MODELS -- DRY AND CLEAN CONDITIONS

A typical 34.5 kV non-ceramic insulator has 12 weather sheds and a length of about 0.8 m. By comparison, a typical 765 kV non-ceramic insulator has over 100 weather sheds and is nearly 5 m long. Therefore, to obtain accurate results, considerably more elements have to be used for the electric field analysis of a 765 kV non-ceramic insulator than for a 34.5 kV non-ceramic insulator. The more elements are used for the boundary element method, the more time is needed for the computations. Therefore, in order to reduce the computation time, some simplifications of the insulator model are necessary.

A non-ceramic insulator, depending on its design, can have up to four main components: the fiberglass reinforced (FRP) rod, the polymeric sheath on the rod, the polymeric weather sheds, and two metallic end fittings. To determine which component can be simplified with the least influence on the accuracy of the calculated results of EFVD, a 34.5 kV non-ceramic insulator is studied for the electric field analysis. Its detailed geometric dimensions are shown in Fig. 1.

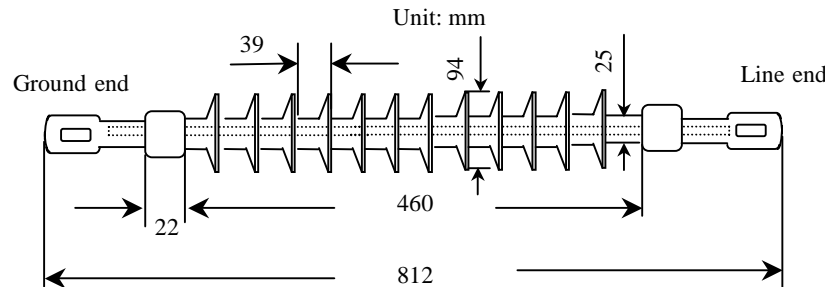


Figure 1: Simplified geometry and dimensions of a typical 34.5 kV non-ceramic insulator used in the computations.

The insulator is equipped with metallic end fittings. It is made of silicon rubber weather sheds with a relative permittivity of 4.3 and a fiberglass rod with a relative permittivity of 7.2. There are 12 weather sheds on the housing. The insulator is surrounded by air with a relative permittivity of 1.0. The top metallic end fitting is taken as the ground electrode and for the purposes of calculations the bottom electrode is

connected to a steady voltage source of 1000 V. The insulator is positioned vertically, but shown horizontally in Fig. 1 for convenience.

Four simplified computation models are used for the step by step comparison process. In addition, a three dimensional “full” insulator model is set up as a reference to study the effects of the four simplified models on the EFVD along the insulator.

These five computation models are: (a) two electrodes only, (b) two electrodes and the fiberglass rod, (c) two electrodes, rod and sheath on the rod without weather sheds, (d) two electrodes, rod, sheath, and two weather sheds at each end of the insulator, (e) the “full” 34.5 kV insulator.

The equipotential contours around the five computation models are shown in Fig. 2. The energizing voltage is 1000 V. The insulation distance between two electrodes is 46 cm.

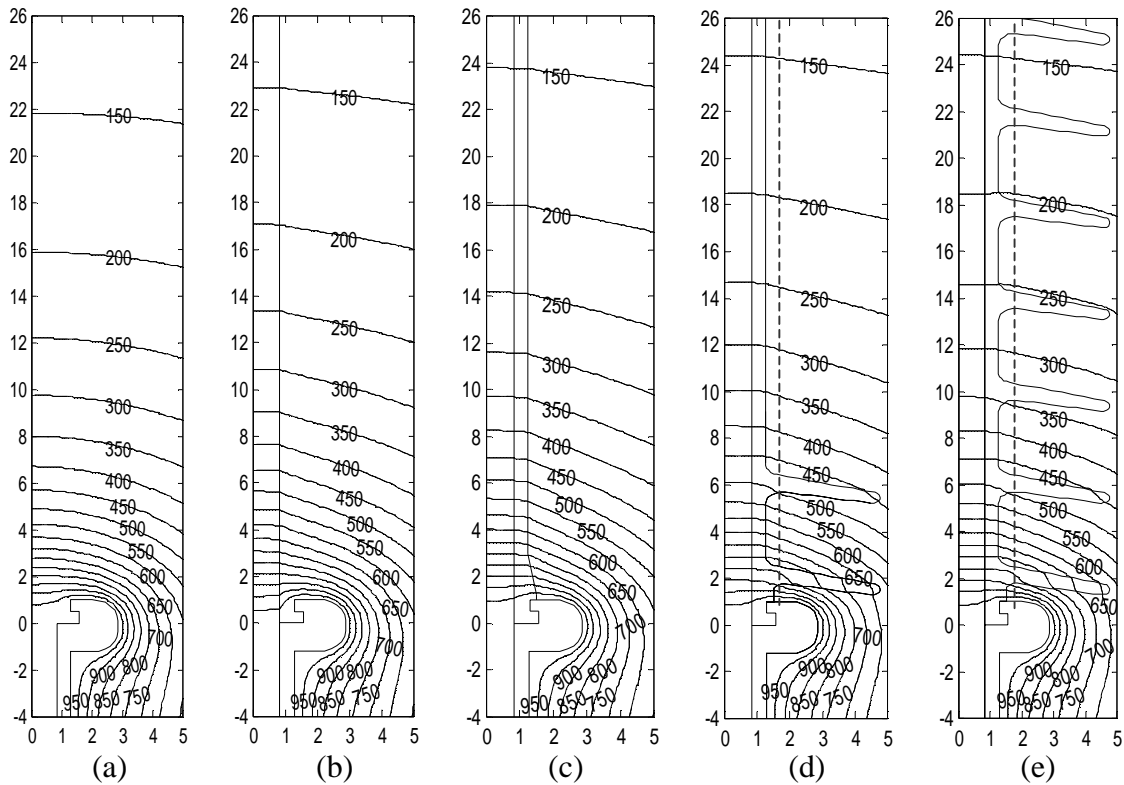


Figure 2: The equipotential contours around the five computation models.

Each number shown along the perimeters of the four contour plots means centimeters. Case (a), no solid insulating material between the electrodes, shows that 20% of the insulation distance sustain about 70% of the applied voltage. The presence of the fiberglass rod changes the voltage distribution slightly, see Case (b). The distribution of the equipotential contours for Case (c), with the sheath on the rod, is very close to Case (e), the “full” insulator model. The presence of the weather sheds changes the equipotential contours somewhat. If more accurate results of voltage distribution are needed near the line and ground end area, the simplified insulator model with two weather sheds at each end of the insulator, Case (d), can be used. If accurate results of the voltage distribution along the entire length of the insulator are needed, then the “full” insulator model, Case (e), is to be used.

Comparing Cases (d) and (e), the voltage distributions in the vicinity of the two weather sheds are very similar to each other. Moreover, the positions of the equipotential lines for Cases (d) and (e) are very close to each other along the sheath surface of the insulator. Comparing Cases (d) and (e), the maximum difference between the voltages at the same point along the sheath surface of the insulator is only 1.2% of the applied voltage. This indicates that the simplification introduced by Case (d) is acceptable for the computation of the voltage distribution of the “full” insulator, Case (e), along the sheath surface.

The electric field strength magnitudes for Cases (d) and (e) along the paths defined on the surface of the sheath are also calculated for comparison, which is shown in Fig. 3. The dips in the electric field strength plot of the insulator modeled with weather sheds are due to the calculation path passing through the weather shed material, which has a relative permittivity of 4.3. The electric field strength in the vicinity of the two weather sheds at each end of the insulator is same for Cases (d) and (e).

There is a slight change in the electric field strength distribution near the other 8 weather sheds shown by Case (e). However, the electric field strength outside the weather sheds region still has a good correspondence in Cases (d) and (e). The maximum electric field strength for Case (d) is 0.0256 kV<sub>p</sub>/mm, and for Case (e) is 0.0256 kV<sub>p</sub>/mm. They are the same, which means that the electric field distribution of the insulator with the “full” number of weather sheds can be estimated through the simplified insulator model with a small number of weather sheds (e.g., 2) at the each end of the insulator.

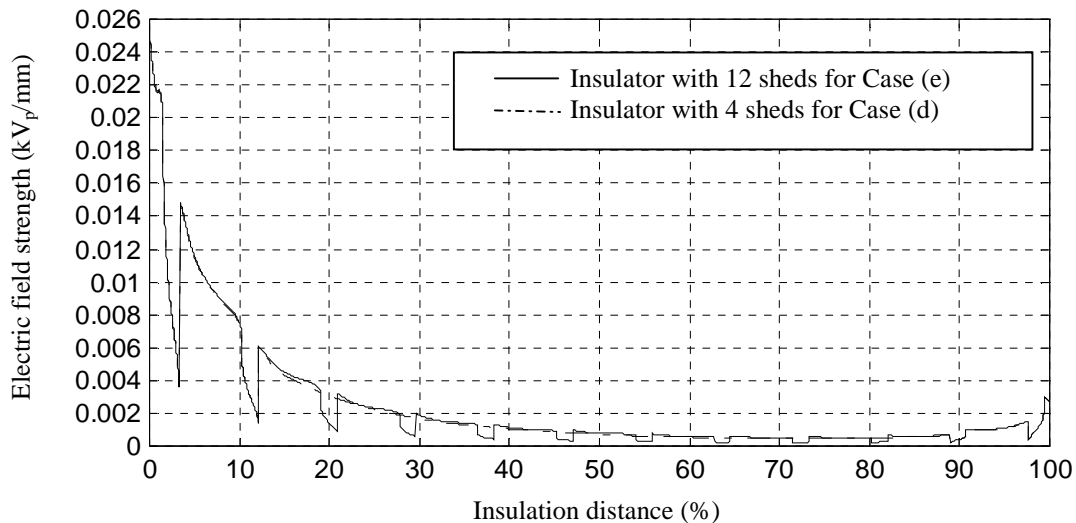


Figure 3: Electric field strength magnitude along the insulation distance at the sheath surface for the “full” insulator, Case (e), and the simplified insulator model, Case (d).

The conclusion is that a simplified insulator model with only a small number of weather sheds can be used to calculate the EFVD along the full insulator in service with no significant effect on accuracy. The number of weather sheds for the simplified insulator model can be decided by trial and error.

### 3. COMPUTATION MODEL OF A 765 kV NON-CERAMIC INSULATOR

It is of practical interest to know the electric field strength distribution for a full-scale insulator under three phase energization. A typical 765 kV non-ceramic insulator is used for this study, which is designed for four sub-conductor bundles. When non-ceramic insulators are installed on a power line, the tower geometry, live-end hardware and conductors in the vicinity of the insulators will have some effects on the electric field distribution around the insulators. Grading rings is also used to redistribute the electric field distribution and reduce the maximum value of the electric field strength. Consequently, to consider all these effects, a three-dimensional calculation model must be set up in the Coulomb software in order to evaluate the EFVD near and along a non-ceramic insulator.

The detailed geometric dimensions of the 765 kV insulator are shown in Fig. 4. The insulator is made of silicon rubber with a relative permittivity of 4.0 and an FRP rod with a relative permittivity of 5.5. There are 51 large and 52 small weather sheds on an actual 765 kV insulator. The insulator is equipped with metal fittings at both line and ground ends. Based on the previous study, the calculation model for this full scale insulator can be simplified with only a small number of weather sheds (e.g., 10) at each end of the insulator in order to calculate the EFVD along the insulator.

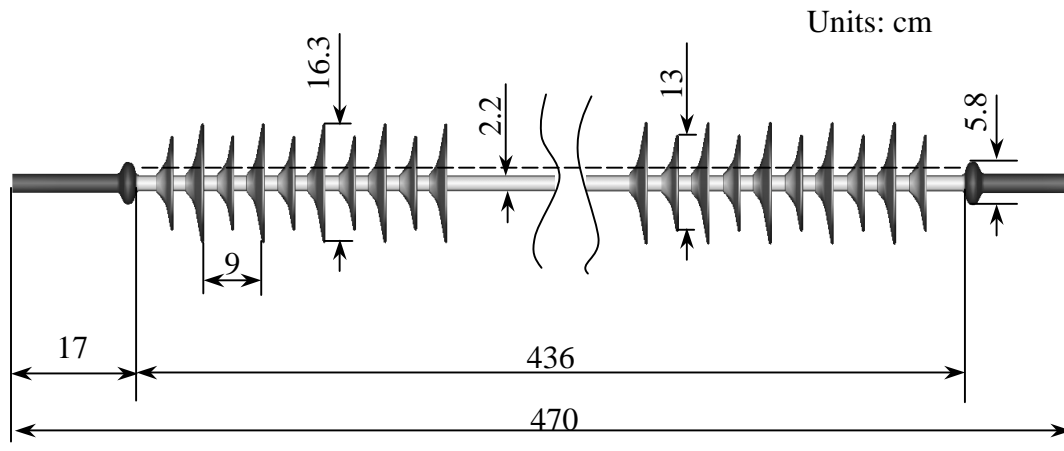


Figure 4: Simplified geometry and dimensions of the 765 kV non-ceramic insulator model with 10 weather sheds at the line end and ground ends.

The simplified geometry and major dimensions of a typical 765 kV power line tower with four-subconductor bundles are shown in Fig. 5. The angle between the center phase insulator and the symmetry line of the tower is  $50^\circ$ , as marked on Fig. 5. The two ground wires are ignored in the calculations. The length of each conductor considered is 60 m. Each conductor is positioned parallel to the ground. The ground plane is modeled as a 50 m by 50 m large plane with zero potential.

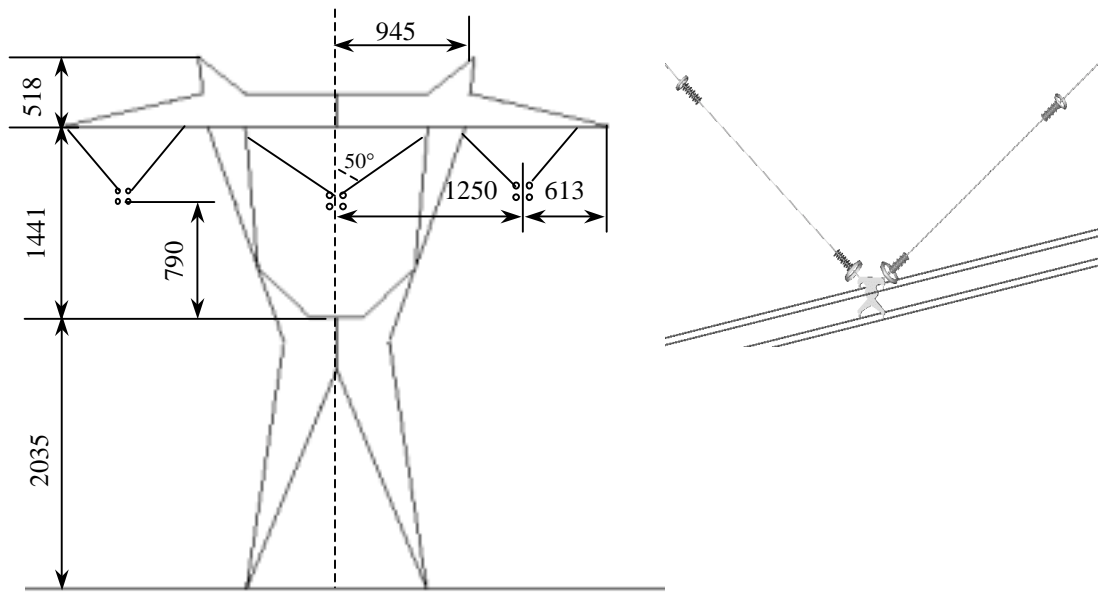


Figure 5: 765 kV power line tower with four-subconductor bundles, dimensions are shown in cm.

The electric field and voltage distributions along the 765 kV non-ceramic insulator of the center phase have been studied on a typical power line tower with four-subconductor bundles.

The instantaneous voltages applied to the three phase conductor system for the worst case when there is maximum voltage across the center phase insulator are:

- $V_{\text{left}} = -0.5 \times V_{\text{center}} = -0.5 \times 624.6 = -312.3 \text{ kV}$ ,
- $V_{\text{center}} = 765 \times \sqrt{2} / \sqrt{3} = 624.6 \text{ kV}$  (i.e., max. value of the line-to-ground voltage),
- $V_{\text{right}} = -0.5 \times V_{\text{center}} = -0.5 \times 624.6 = -312.3 \text{ kV}$ .

There are some basic principles for showing the calculation results:

- In the following paragraphs, the voltages are expressed either in  $\text{kV}_p$  or in per cent values, referred to  $624.6 \text{ kV}_p$ , which is the actual applied voltage on the center phase insulator.
- The electric field strength is always expressed in  $\text{kV}_p/\text{mm}$  units.
- The insulation distances used in the figures are expressed either in cm units or in per cent values, referred to 436 cm as shown in Fig. 4.
- The calculation path on the surface of the insulator sheath is identified as a straight dashed line as shown in Fig. 4 (not along the leakage path).

The resulting per cent equipotential contours inside the tower window for a 765 kV non-ceramic insulator with a four-subconductor bundle are shown in Fig. 6.

It can be seen that the line end equipotential contours are greatly influenced by the line-end hardware and the line-end corona ring and are nearly parallel to the shed surface. The ten weather sheds near the line end sustain about 35% of the applied voltage. The ten weather sheds near the ground end sustain about 12% of the applied voltage.

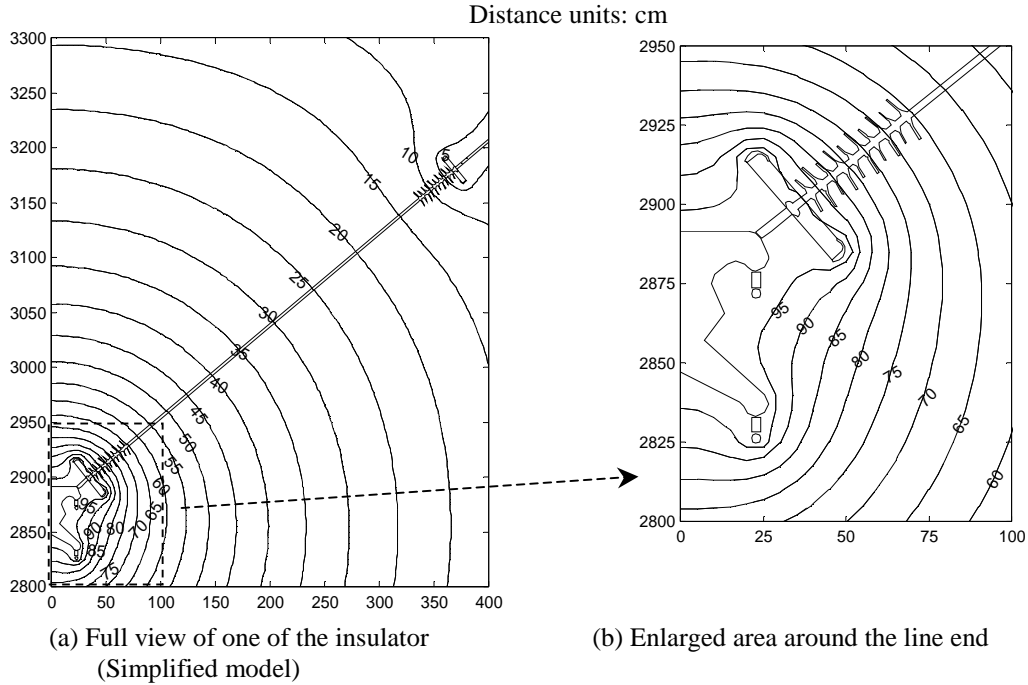


Figure 6: Per cent equipotential contours for a 765 kV tower with four-subconductor bundles under three phase energization.

The electric field strength magnitude along the path defined on the surface of the insulator sheath is shown in Fig. 7. The maximum value of the electric field strength at the triple junction point is  $1.586 \text{ kV}_p/\text{mm}$ . For a clearer view, details of the electric field strength distribution along the insulation distance near the line-end fitting are shown in Fig. 8. The discontinuities in the magnitude of the electric field strength in Figs. 7 and 8 are the result of the calculation path, shown in Fig. 4, passing through the shed material, which has a relative permittivity of 4.0. It can be seen that electric field strength is much higher at the junction region between the sheath and the shed than that at the middle part of the sheath region.

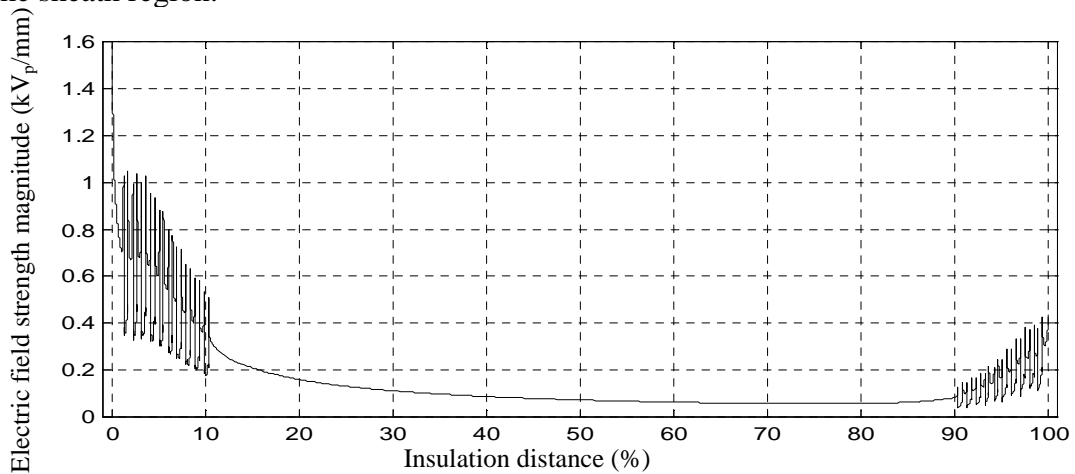


Figure 7: Electric field strength magnitude vs. per cent insulation distance at the surface of the insulator sheath with four-subconductor bundles.

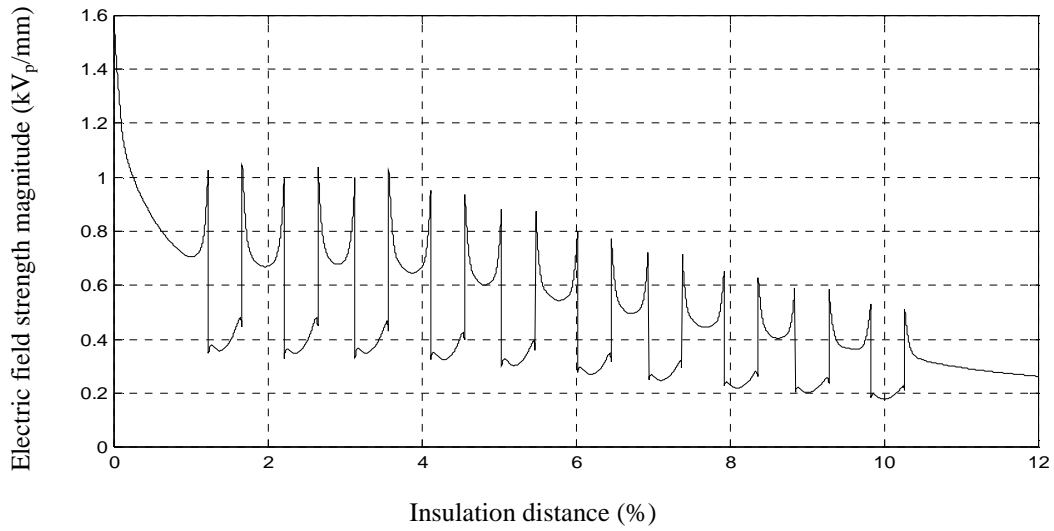


Figure 8: Electric field strength magnitude vs. per cent insulation distance at the surface of the insulator sheath with four-subconductor bundles near the line end.

The electric field strength distribution along the insulation distance near the ground end fitting is also shown in Fig. 9.

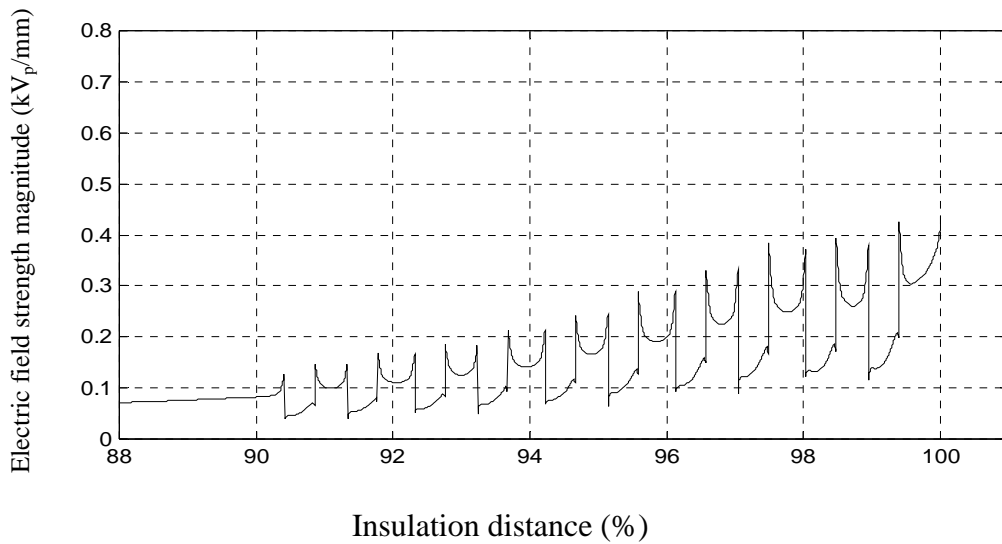


Figure 9: Electric field strength magnitude vs. per cent insulation distance at the surface of the insulator sheath with four sub-conductor bundles near the ground end.

#### 4. INSULATOR COMPUTATION MODELS -- WET CONDITIONS

The excellent pollution performance of non-ceramic insulators is due to the good hydrophobic surface property of weather sheds under wet and contaminated conditions. During the service life of an insulator, the combined effects of electric and environmental stresses accelerate the aging of the non-ceramic insulators. Consequently, the hydrophobicity properties of non-ceramic weather sheds will be temporarily or permanently lost.

Under rain and fog conditions, the presence of water droplets intensifies the electric field strength on the surface of a non-ceramic insulator. The study of the EFVD along the non-ceramic insulators is important for the in-depth understanding of the aging process and the pollution flashover initiation mechanism.

Assuming a vertical suspension insulator, there are sessile water droplets on the weather sheds, clinging water droplets on the vertical surface of the polymer sheath of the insulator and pendant water droplets under the sheds. The surface of the insulator shed is close to parallel to the equipotential lines. The surface of the sheath is close to perpendicular to the equipotential lines.

As the first step, two simple models have been set up to study the basic features of the electric field distribution around water droplets. In both models, a flat hydrophobic silicone rubber sheet with one discrete water droplet between two electrodes is used to study the electric field enhancement in the vicinity of water droplets. One electrode is energized (e.g., 100 Volts), the other one is grounded. The software used assumes a “remote” ground as well. It is equivalent to conducting an experiment in a high voltage laboratory with the floor, ceiling and walls grounded.

In order to represent the sheath region, two electrodes are considered together with a single SiR sheet between them. This case is shown by Fig. 10. In order to represent the shed region, the SiR sheet is positioned parallel between the two electrodes. This arrangement is shown by Fig. 13.

### **a. Sheath Region Simulation**

In order to represent the sheath region of an insulator, two electrodes are assumed together with a single SiR sheet. The size of the SiR sheet is 10 cm × 10 cm and it is 0.5 cm thick. The relative permittivity of the SiR material used in the calculation is 4.3. The two electrodes are positioned at 10 cm distance from each other. The position of the SiR sheet is shown in Fig. 10; the SiR sheet is between the two electrodes as a spacer to simulate the sheath region. The energized electrode is on the left side and the grounded electrode is on the right side. The applied voltage is 100 V, which means the average electric field strength is  $100/10=10$  V/cm. The x, y, z directions are defined as shown in Fig. 10.

A water droplet of hemispherical shape is assumed at the midway of the electrode spacing. The diameter of the water droplet is 4mm and its height is 2 mm. The relative permittivity of the water droplet is 80 and its conductivity is assumed to be zero.

The enlarged view of the equipotential contours and electric field lines around the water droplet positioned on a SiR sheet simulating the sheath region is shown in Fig. 11. Continuous lines represent the equipotential contours; dashed lines are used for the electric field lines. It can be seen from Fig. 11 that the presence of the water droplet

causes a considerable distortion in the configuration of the equipotential contours and the electric field lines in the vicinity of the water droplet. For the sheath region simulation, the electric field strength is significantly increased at the interface of the water droplet, air, and the insulating sheet.

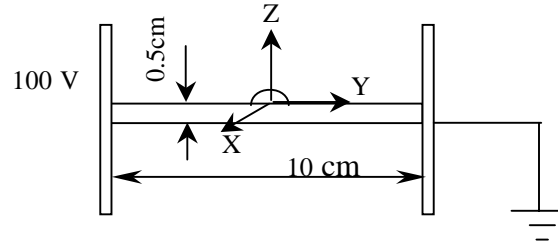


Figure 10: Experimental setup for the sheath region simulation.

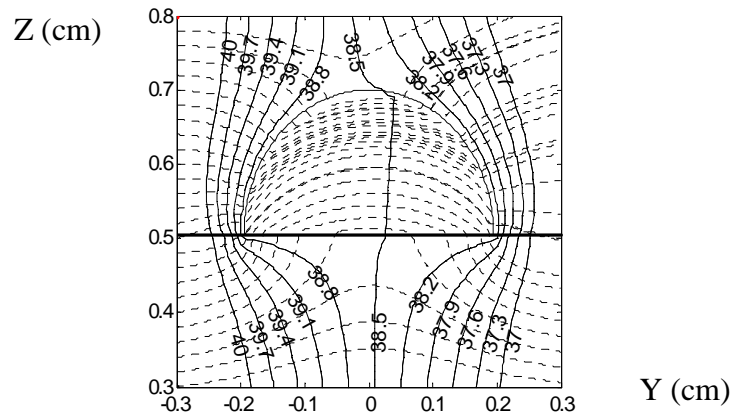


Figure 11: Equipotential contours and electric field lines around a water droplet on the sheath surface.

The electric field strength vector changes its magnitude and direction along the surface of the water droplet. To follow its changes, several quantities can be monitored, for example, the x, y, or z components of the electric field strength vector, or the magnitude of the electric field strength vector. The x, y, z, components and the magnitude of the electric field strength on the surface of the water droplet on the sheath region are shown in Fig. 12 (a), (b), (c), (d), respectively. Each point on the surface of the water droplet is described by its three coordinates (x, y, z). In fact, a fourth dimension would be needed to show the distribution of the magnitude of the electric field strength.

In order to be able to show the electric field strength distribution on the surface of the water droplets using a 3D graph, the surface point is represented by its (x,y) coordinates only. In other words, all points on the surface of the water droplet are represented by their projection in the (x,y) plane. Then the z dimension can be used to show the magnitudes of the electric field strength vector or its components at any point on the surface of the water droplet.

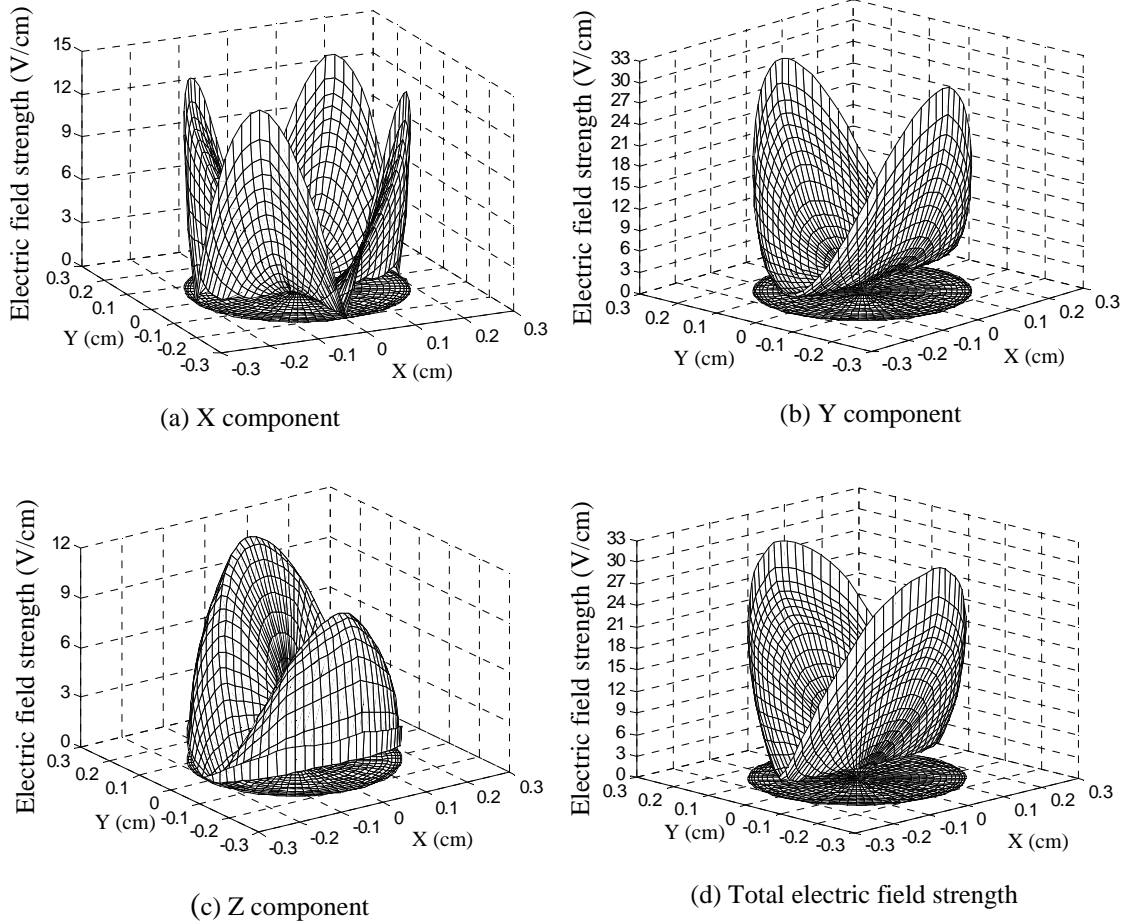


Figure 12: Vector components and the magnitude of the electric field strength on the surface of the water droplet on the sheath surface.

For a water droplet in the sheath region, the maximum value of the electric field strength, at 100 V applied voltage, is 32.9 V/cm on the surface of the water droplet, at the interface of the water droplet, air and insulating material. The electric field enhancement factor is 3.29, which is defined as the ratio of the maximum electric field strength at the tip of the water droplet and the average applied field strength under dry conditions without the water droplet (10 V/cm). The y component of the electric field strength vector is the dominant component, as expected.

### b. Shed Region Simulation

In order to represent the shed region of an insulator, two electrodes are assumed together with a single SiR sheet. The two electrodes are positioned at 10 cm distance from each other. The SiR sheet is in a parallel position between the two electrodes for simulating the weather shed region as shown in Fig. 13. The upper electrode is energized and the lower electrode is grounded. The applied voltage is 100 V, which means the

average electric field strength is  $100/10=10$  V/cm. The x, y, z directions are defined as shown in Fig. 13.

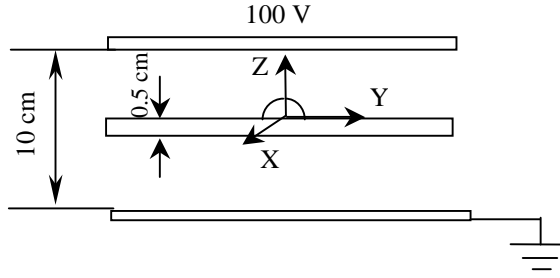


Figure 13: Experimental setup for the shed region simulation.

The enlarged view of the equipotential contours and electric field lines around the water droplet positioned on a SiR sheet simulating the shed region is shown in Fig. 14. Continuous lines represent the equipotential contours; dashed lines are used for the electric field lines. It can be seen from Fig. 14 that the presence of the water droplet causes a considerable distortion in the configuration of the equipotential contours and the electric field lines in the vicinity of the water droplet. For the shed region simulation, the electric field strength is enhanced at the top of the water droplet.

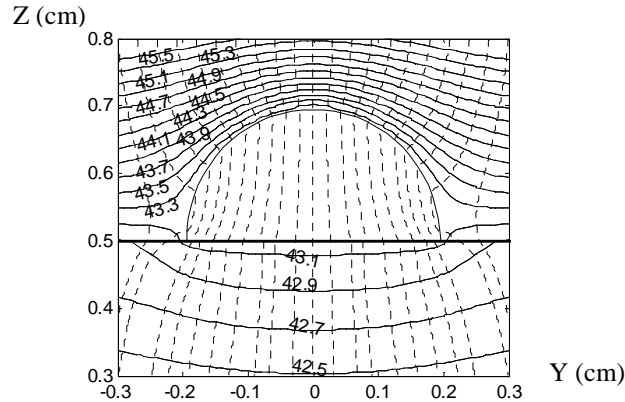


Figure 14: Equipotential contours and electric field lines around a water droplet on the shed surface.

The x, y, z, components and the magnitude of the electric field strength on the surface of the water droplet on the sheath region are shown in Fig. 15 (a), (b), (c), (d), respectively. Similarly to the sheath region simulation, all points on the surface of the water droplet are represented by their projection in the (x,y) plane. Then the z dimension can be used to show the magnitudes of the electric field strength vector or its components at any point on the surface of the water droplet.

For a water droplet in the shed region, the maximum value of the electric field strength, at 100 V applied voltage, is 27.6 V/cm on the top of the water droplet. The electric field enhancement factor is 2.76. The z component of the electric field strength vector is the dominant component, as expected.

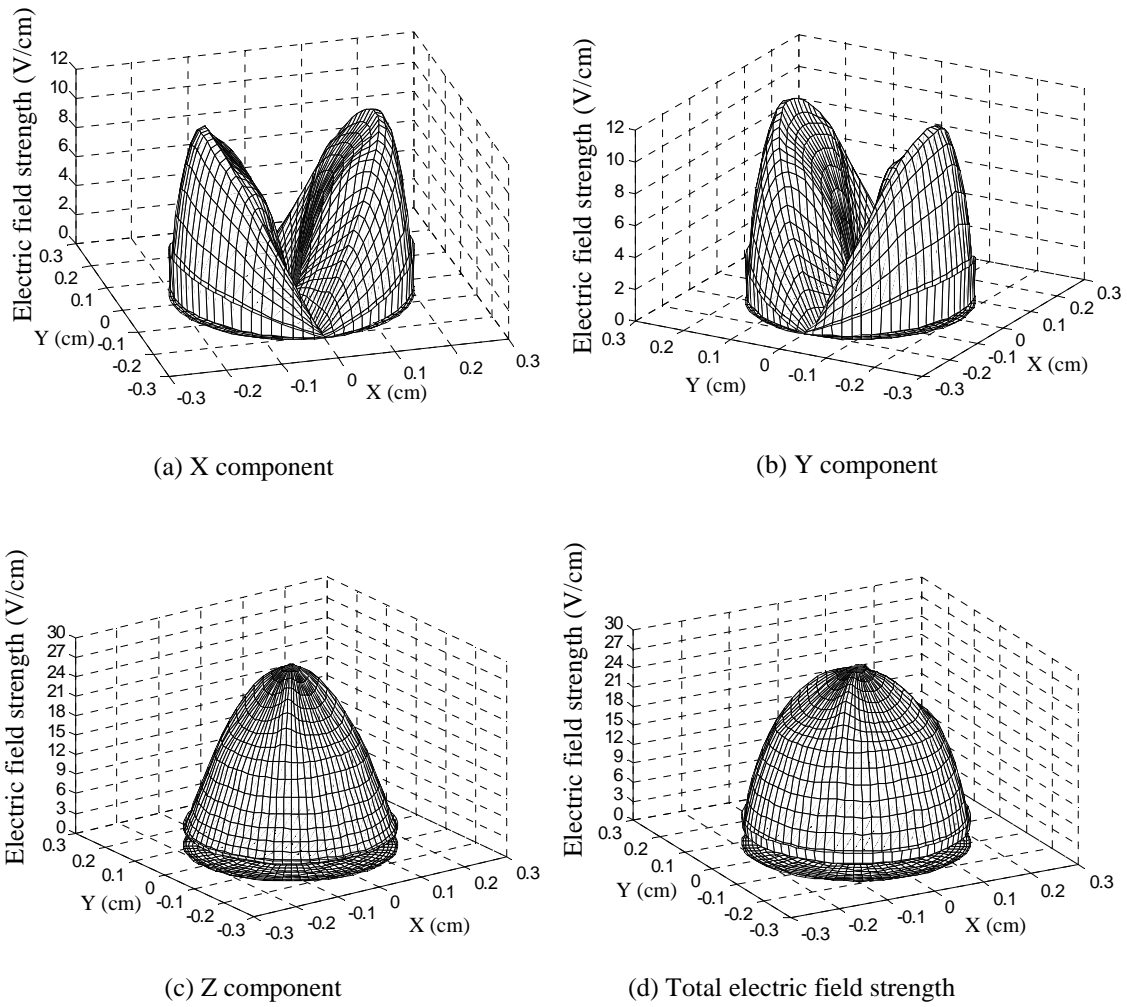


Figure 15: Vector components and the magnitude of the electric field strength on the surface of the water droplet on the shed surface.

## 5. ANALYSIS OF THE EFVD UNDER RAIN AND FOG CONDITIONS

The test geometry considered for the following calculations is a short insulator with only four weather sheds. The simplified geometry and dimensions of the non-ceramic insulator to be modeled are shown in Fig. 16.

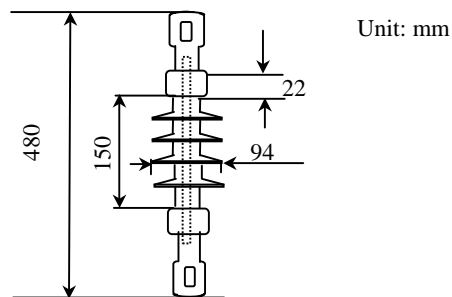


Figure 16. Geometry and dimensions of a four-shed non-ceramic insulator.

In order to reduce the calculation time, only a 10 degree segment of the weather shed surfaces is modeled. The applied voltage at the line end is 100 V.

The following three models are used for simulating specific weather conditions:

- The dry and clean model: the insulator is identical to the shape of the non-ceramic insulator.
- The "rain" model: seven water droplets are assumed on each 10 degree segment of each weather shed. That means  $7 \times 36 = 252$  water droplets on each shed, and  $252 \times 4 = 1008$  water droplets on the four weather sheds of the insulator. The shape of all water droplets is hemispherical, with a diameter of 2mm. The relative permittivity of the water droplets is 80 and their conductivity is  $50 \mu\text{S} / \text{cm}$ . The surface of the vertical sheath and the undersides of the sheds are dry.
- The "fog" model: the water droplet distribution is similar to that of the "rain" model, the only difference is that the undersides of the sheds are covered by a continuous water film layer. The relative permittivity of the water droplets is 80 and their conductivity is  $250 \mu\text{S} / \text{cm}$  for this case.

The equipotential contours of the three models are shown in Fig. 17. Fig. 17(a) shows (as expected) the non-uniform electric field distribution along a dry and clean insulator.

Fig. 17(b) shows that assuming the "rain" model conditions, the electric field strength around the bottom weather shed area is slightly less than in the dry and clean case. The presence of the water droplets on the top surface of the weather sheds makes the overall electric field distribution a bit more uniform than the dry case. (Of course, the local electric field strength in the vicinity of each water droplet is enhanced.) As a result, the overall electric field strength around the triple junction area (housing, air, and line-end metal fitting) is a bit less than in the dry and clean case. Finally, Fig. 17(c) shows that assuming the "fog" model conditions, the dry areas along the sheath sections of the insulator sustain most of the voltage. The overall electric field strength along the bottom area of the insulator is significantly higher than in the dry and clean case.

## 6. CONCLUSIONS

The electric field strength and voltage distributions (EFVD) around non-ceramic insulators have been studied and illustrated for several cases using the COULOMB software.

- Various computational models developed for the study of dry and clean non-ceramic insulators have been compared in terms of efficiency and accuracy. The results show that a significant number of weather sheds can be omitted and the accuracy of the calculations is still acceptable.
- Various aspects of the EFVD of a 765 kV non-ceramic insulator have been examined for three phase energization.
- The EFVD around a hemispherical water droplet in two different positions has been calculated. The degree of electric field enhancement has been calculated.

- The overall electric field distribution along a non-ceramic insulators appears to be more uniform for "rain" than for dry and clean conditions.
- The dry area along the sheath sections sustain most of the voltage for the "fog" conditions assumed.

## 7. ACKNOWLEDGMENT

The support of Mr. Craig Armstrong, General Manager of Integrated Engineering Software, was invaluable for this study.

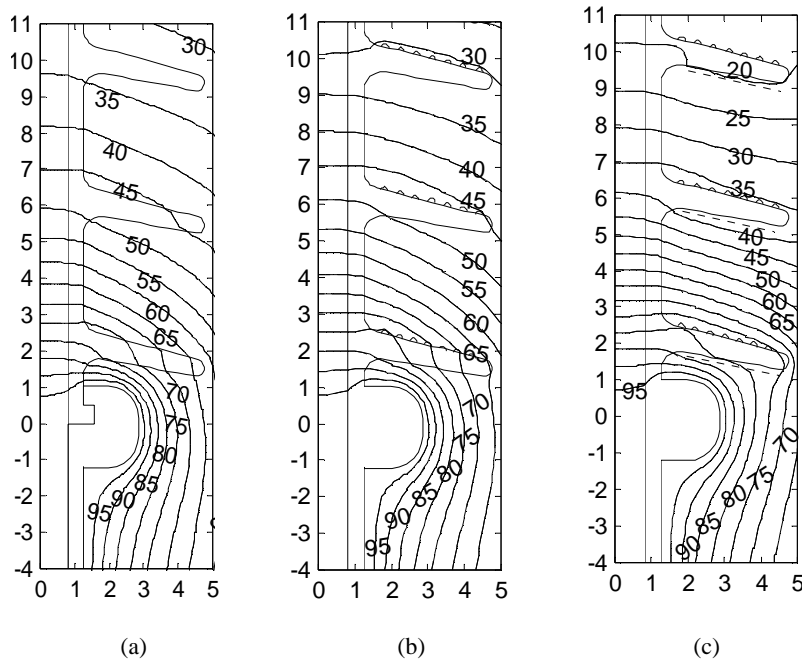


Figure 17: Equipotential contours for (a) dry and clean model, (b) "rain" model, (c) "fog" model.

## 8. REFERENCES

[1] A. J. Phillips, D. J. Childs, H. M. Schneider, " Aging of Non-Ceramic Insulators due to Corona from Water Drops," *IEEE Transactions on Power Delivery*, Vol. 14, No. 3, pp. 1081-1088, July 1999.

## AUTHORS' ADDRESSES

**Weiguo Que**, Axcelis Technologies, 108 Cherry Hill Drive, Beverly, MA 01915, USA, weiguo.que@axcelis.com

**Stephen A. Sebo**, Department of Electrical Engineering, The Ohio State University, Columbus, OH 43210-1272, USA, sebo.1@osu.edu